ARL-TR-7531 ● Nov 2015

US Army Research Laboratory

# Tensile Deformation and Adiabatic Heating in Post-Yield Response of Polycarbonate

by C. Allan Gunnarsson, Bryan Love, Paul Moy, and Tusit Weerasooriya

## NOTICES

### Disclaimers

The findings in this report are not to be construed as an official Department of the Army position unless so designated by other authorized documents.

Citation of manufacturer's or trade names does not constitute an official endorsement or approval of the use thereof.

Destroy this report when it is no longer needed. Do not return it to the originator.

ARL-TR-7531 ● Nov 2015

US Army Research Laboratory

# Tensile Deformation and Adiabatic Heating in Post-Yield Response of Polycarbonate

**by C. Allan Gunnarsson, Bryan Love, Paul Moy, and Tusit Weerasooriya**

***Weapons and Materials Research Directorate, ARL***

# REPORT DOCUMENTATION PAGE

*Form Approved*
*OMB No. 0704-0188*



| 1. REPORT DATE *(DD-MM-YYYY)* | 2. REPORT TYPE | 3. DATES COVERED (From - To) |
|---|---|---|
| November 2015 | Final | January 2014–August 2015 |

**4. TITLE AND SUBTITLE**
Tensile Deformation and Adiabatic Heating in Post-Yield Response of Polycarbonate

**5a. CONTRACT NUMBER**

**5b. GRANT NUMBER**

**5c. PROGRAM ELEMENT NUMBER**

**6. AUTHOR(S)**
C Allan Gunnarsson, Bryan Love, Paul Moy, and Tusit Weerasooriya

**5d. PROJECT NUMBER**

**5e. TASK NUMBER**

**5f. WORK UNIT NUMBER**

**7. PERFORMING ORGANIZATION NAME(S) AND ADDRESS(ES)**
US Army Research Laboratory
ATTN: RDRL-WMP-B
Aberdeen Proving Ground, MD 21005-5069

**8. PERFORMING ORGANIZATION REPORT NUMBER**
ARL-TR-7531

**9. SPONSORING/MONITORING AGENCY NAME(S) AND ADDRESS(ES)**

**10. SPONSOR/MONITOR'S ACRONYM(S)**

**11. SPONSOR/MONITOR'S REPORT NUMBER(S)**

**12. DISTRIBUTION/AVAILABILITY STATEMENT**
Approved for public release; distribution is unlimited.

**13. SUPPLEMENTARY NOTES**

**14. ABSTRACT**
It is well known that amorphous polymers, such as polycarbonate (PC), will exhibit adiabatic heating due to the large plastic work that occurs when undergoing significant plastic deformation. However, the extent of adiabatic heating has not been investigated, with respect to strain rate, with full-field temperature measurements performed on the specimen during deformation. In this study, American Society for Testing and Materials tensile dog-bone PC specimens were used to investigate the rate-dependent mechanical response from quasi-static to intermediate (~5/s) strain rates using a traditional servo-hydraulic load frame. To determine the variations in yield and post-yield response at different locations of the gage area of the specimen, digital image correlation was used to measure the full-field surface strains. In addition, an InSb thermal camera was used concurrently to measure the full-field temperature distribution in the gage area during the deformation. The material experienced nonuniform temperature increases as high as 30 °C and showed significant rate-sensitive mechanical response.

**15. SUBJECT TERMS**
polycarbonate, tension, rate effects, thermal, heating

| 16. SECURITY CLASSIFICATION OF: | | | 17. LIMITATION OF ABSTRACT | 18. NUMBER OF PAGES | 19a. NAME OF RESPONSIBLE PERSON |
|---|---|---|---|---|---|
| a. REPORT | b. ABSTRACT | c. THIS PAGE | | | C Allan Gunnarsson |
| Unclassified | Unclassified | Unclassified | UU | 22 | 19b. TELEPHONE NUMBER (Include area code) 410-306-0990 |

## Contents

**List of Figures** **iv**

**1. Introduction** **1**

**2. Experiments** **2**

**3. Results** **3**

3.1 Strain-Rate-Dependent Necking Behavior 3

3.2 Low-Rate Mechanical Behavior 4

3.3 Intermediate-Rate Mechanical Behavior 6

3.4 Rate Effects on Mechanical Behavior 8

3.5 Thermal Behavior 8

**4. Conclusions** **13**

**5. References** **14**

**List of Symbols, Abbreviations, and Acronyms** **16**

**Distribution List** **17**

## List of Figures


Fig. 1 ASTM D638.10 plastic tensile specimen geometry (for less than 7-mm thickness)....2

Fig. 2 Graphical a) and DIC b) representation of quasi-static tensile behavior of PC....3

Fig. 3 a) Locations of strain history extraction and b) strain history as a function of time....4

Fig. 4 Strain history as a function of time (max and gage length only)....5

Fig. 5 Mechanical response of PC at quasi-static rate for a) all locations and b) gage length average and maximum only....6

Fig. 6 Mechanical response of PC specimen at intermediate rate....7

Fig. 7 Intermediate a) strain histories for max and gage length and b) stress-strain behavior of PC at intermediate rate for max and gage length....7

Fig. 8 Mechanical response at quasi-static and intermediate strain rate for PC....8

Fig. 9 Quasi-static a) thermal distribution and b) temperature and strain history at 0.001/s for PC....9

Fig. 10 Distribution profiles along the gage length for PC at quasi-static rate for a) strain and b) temperature change....10

Fig. 11 Cooling response of PC specimens after failure....11

Fig. 12 Maximum temperature change and strain histories for PC at a) quasi-static and b) intermediate rates....12

Fig. 13 Maximum temperature change as a function of max strain for PC at a) quasi-static rate and b) intermediate rate....12

## 1. Introduction

Polycarbonate (PC) is an amorphous glassy polymer that is widely used for transparent protection. These materials are found in applications for the military, aerospace, and automotive industries, safety glasses, and household windows. The advantages of these classes of amorphous glassy polymers are being lightweight and having exceptional clarity as well as their ability to be molded into various shapes and sizes. In addition to these properties, these polymers are used in applications where impact resistance is important because of their high impact strength characteristics.

PC is a thermoplastic polymer that is easily molded and thermoformed with a density of about 1.2 g/cm$^3$. This is due in part to the low glass transition temperature ($T_G$) of 150 °C and melting point of about 267 °C.[1,2] The $T_G$ is the temperature at which an amorphous solid, such as glass or a polymer, becomes solid on cooling or soft on heating.[3] PC has been extensively investigated for its toughness and tensile and compressive strengths. The mechanical properties of polymers depend upon 2 key factors, the rate of deformation and the material temperature. Polymers typically exhibit an increase in the yield strength and modulus and a decrease in strain to failure as the strain rate increases from quasi-static (~$10^{-3}$/s) to dynamic ($10^3$/s).[4,5]

Research by Moy et al.[6] showed that PC is rate-sensitive under uniaxial compression. They reported a softening after yielding followed by a strain hardening phase at low and high strain rates. Mulliken and Boyce[7] reported similar behavior of PC at high strain rates. Their work also included dynamic mechanical analyses for PC and poly(methyl methacrylate), or PMMA, to characterize the visco-elastic behavior for these thermoplastics. Another polymer study by Hall[8] reports that the temperature increases during deformation at high strain rate while no appreciable temperature change occurs during deformation at lower rates. Research by Walley et al.[9] has shown that the strain rate and temperature affect the strain hardening behavior of glassy polymers. For both PC and PMMA, Arruda et al.,[10] Boyce et al.,[11] and Boyce and Sarva[12] have proposed material models to predict the deformation response for differing strain rates.

In this study, the tensile mechanical behavior of PC is studied as a function of strain rate between quasi-static (0.001/s) and intermediate (~5/s) strain rates with a focus on the behavior after yield. Optical strain measurement techniques, including digital image correlation (DIC), were used to measure the strain distribution and identify areas of localized plastic strain concentration (necking). DIC is a widely used technique to make detailed deformation and displacement measurements of

materials and systems.[13–17] In addition, as the specimens yielded and plastic deformation occurred, adiabatic heating also occurred, with the largest amount of heat generation localized at the plastic deformation concentration (necking). A thermal, or infrared (IR), camera was used to measure the temperature change and heat generated in the specimen at both rates. This allowed for the effect of strain rate on adiabatic heat generation to be quantified.

## 2. Experiments

ASTM D638-10[18] standard polymer tensile dog-bone specimens were cut out of 5.75-mm-thick PC sheet by waterjet. The specimen geometry is shown in Fig. 1 (in millimeters). The specimen edges were hand polished using wetted 600-grit sandpaper, which ensured that there were no edge or machining effects contributing to premature failure of the specimens. After polishing, no edge marks, nicks, or machining lines were observable (to the naked eye) along the gage length edges.

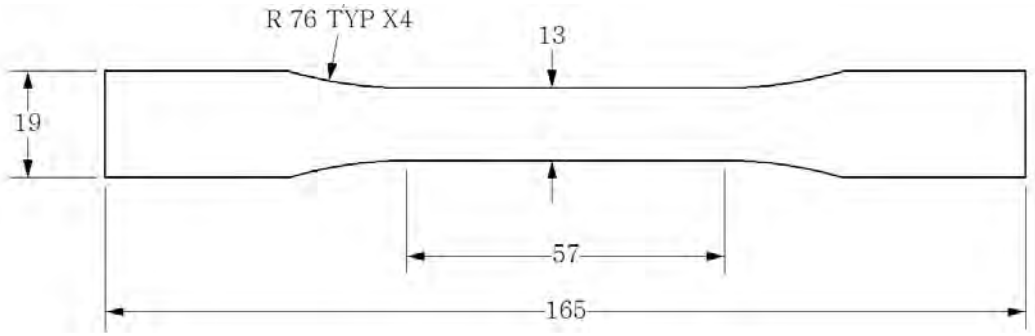


**Fig. 1 ASTM D638.10[18] plastic tensile specimen geometry (for less than 7-mm thickness)**

These specimens were loaded in tension using an Instron servo-hydraulic test frame. Far-field load and stress measurements were made using the load cell installed on the test frame. The specimens were speckled with a random, high-contrast paint pattern to enable the use of DIC to perform direct surface strain measurements. This provided detailed strain distribution data over the entire specimen gage length including strain concentrations that occurred during necking. True stress calculation was made using the global engineering stress and the true (log) strain measurement converted to engineering strain. In addition to performing strain measurements, a forward-looking IR thermal camera, based on an InSb imaging chip, was used to make detailed temperature measurements of the specimen gage length during deformation. These measurements were performed on the unpainted side of the specimen. The experiments were controlled at a constant displacement rate; these rates were chosen to cause average deformation of the specimen at specified strain rates. This is an approximation at best, however. After

yielding, the strain field was not constant across the gage length and the neck position did not remain constant. These difficulties will be discussed in Section 3.

# 3. Results

## 3.1 Strain-Rate-Dependent Necking Behavior

At low, or quasi-static, strain rate (~$10^{-3}$/s), the tensile specimens exhibited ductile behavior; that is, they elastically deformed, yielded, and began to neck at a location within the gage length. However, unlike traditional materials, the neck reached a strain of about 55% and remained constant. Then the neck "spread out" along the entire gage length. After the neck had spread along the entire gage length, plastic strain in the gage section again increased, evenly distributed over the now "fully necked" gage length. Once this plastic strain became large enough, a flaw or defect allowed for a tear to begin. Shortly thereafter, the specimen failed in a brittle fracture, in that there was no evidence of (a second) necking at the point of failure. Additionally, the fracture surfaces were flat, further supporting a brittle failure. This behavior is illustrated graphically in Fig. 2a (the dimensions are not to scale and some are exaggerated so that the behavior is clear). Further, a series of specimen pictures taken during a tensile experiment with strain field data overlaid are shown in Fig. 2b, reinforcing this behavior.

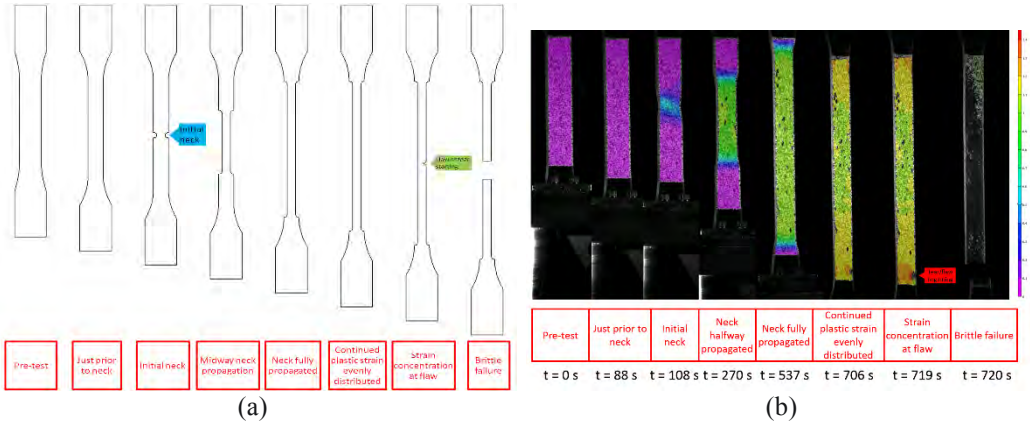


(a) (b)

**Fig. 2 Graphical a) and DIC b) representation of quasi-static tensile behavior of PC**

These quasi-static experiments contrasted the behavior of the PC when loaded in tension at the intermediate strain rate of 5/s where this "neck spreading" behavior was not observed. The PC yielded and plastic strain concentrated into a neck region where strain concentrated until failure.

## 3.2 Low-Rate Mechanical Behavior

Obtaining the mechanical behavior at the low strain rate is difficult because the strain concentration location changes along the length of the specimen as the specimen is stretched. To compare what the strain data look like as a function of location, the strain history was extracted from several locations' average over the entire specimen gage length. The specimen was also divided up into thirds (top, middle, and bottom) and the average strain over each third was extracted. Strain histories were also extracted from the initial neck region and the failure region. Finally, the maximum (max) strain value (wherever it was located on the specimen) was extracted for each data point. The location of this max strain value changed as the strain concentration location changed. However, as can be seen in Fig. 3b, the max strain history (gray) was very similar to the strain history at the initial neck (red). The 2 only diverged just prior to failure, as the strain concentrated at the failure initiation location, which was away from the initial neck location. The locations of these are shown in Fig. 3a, though not shown is max strain, as its location changed. The strain history data from a single experiment for each of these locations is shown in Fig. 3b.

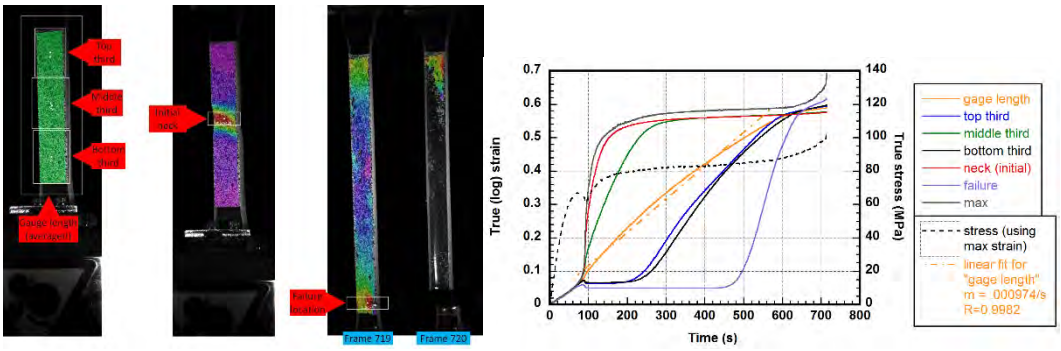


(a) (b)

**Fig. 3 a) Locations of strain history extraction and b) strain history as a function of time**

The strain rate for each specimen is obtained from the post-yield response from the main linear region of the averaged gage length response (orange curve), as this post-yield response is the main focus. The slope is taken as the strain rate; for the experiment shown in Fig. 3b, the strain rate was 0.000974/s, or about $10^{-3}$/s. This is an imperfect way to represent strain rate; after yield, the specimen is not in a state of uniform strain. In addition, the location of strain concentration is changing, and the strain histories from different locations can be quite different and nonlinear.

To illustrate this, the strain histories for only the max and average locations are shown in Fig. 4. The strain rate of the max strain (gray) at the neck is about $10^{-2}$/s during necking (~80–120 s) and then levels off to about $10^{-4}$/s as the neck spreads

out (~140–600 s). This is in contrast to the strain rate measured for the averaged gage length, which remains relatively constant over the entire experiment at approximately $10^{-3}$/s.

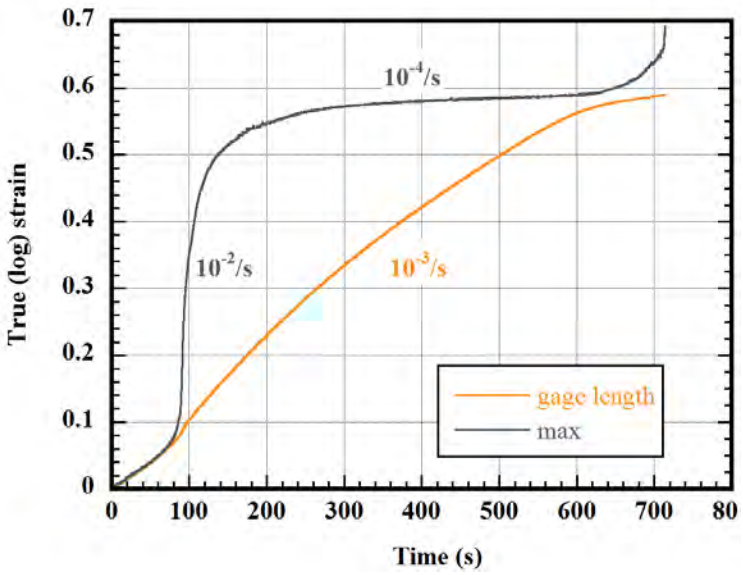


**Fig. 4 Strain history as a function of time (max and gage length only)**

However, there must be some way to represent the differences in deformation rate, especially as the rate progresses from quasi-static (slow Instron testing) to dynamic levels (Kolsky bar testing) and higher. Using the averaged gage length strain to determine a strain rate will provide distinctions between these deformation rates and have 2 other benefits. First, it will allow for compliance with ASTM reporting standards, as these call for the use of a single extensometer to acquire strain data. Averaging the DIC strain over the entire gage length provides similar results to the use of strain gages (small strain) or gage length extensometers (large strain). Second, using an averaged gage length strain rate will allow the results to be compared with previous research that did not have the additional information or detail provided by full-field strain measurements.

These data can also be shown with loading history to obtain the mechanical (stress-strain) response of the specimen, as shown in Fig. 5. Although there is significant variation in the strain histories (Fig. 3b), there is not a tremendous difference between the stress-strain data based on extraction location. The biggest variation is just after yielding, where the level of softening depends on the strain data extraction location. The elastic behavior, modulus, and yield stress (as to be expected due to state of strain uniformity), as well as the later strain-hardening behavior, are all very similar regardless of strain extraction location.

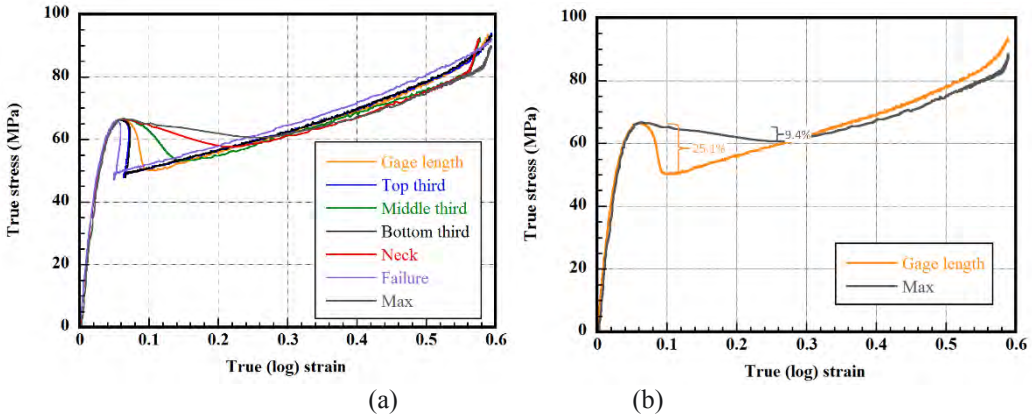


**Fig. 5 Mechanical response of PC at quasi-static rate for a) all locations and b) gage length average and maximum only**

The results from previous studies resemble the data shown in Fig. 5, using the averaged gage length as the location to extract strain, in that they show a significant softening that occurs just after yield. This is to be expected, as those studies used an extensometer to measure strain as the standard dictates, averaging the strain in the specimen over the entire gage length. However, using the actual maximum strain in the specimen is a more accurate way to represent the intrinsic material mechanical behavior because it measures and accounts for the strain concentration that occurs during necking.

The large drop in stress between yield and the point when strain hardening begins has been previously attributed to a softening that occurs in the material as adiabatic heating begins during plastic straining of the specimen. However, using the max strain as a measure of the strain history of the specimen shows that this softening behavior may not be as influential as previously thought. This is illustrated in Fig. 5b, which compares the mechanical response of the PC for only the averaged gage length strain and max strain histories. Note the difference in the level of decreased stress during the softening region; the averaged gage length shows a drop of 16.8 MPa, or 25.1% of yield stress (67 MPa), while the max strain shows a drop of only 6.3 MPa, which is 9.4% of yield stress.

## 3.3 Intermediate-Rate Mechanical Behavior

At the intermediate strain rate (~5/s), the mechanical behavior was more traditional; the specimens would yield, neck, and eventually fail in the neck. This makes interpretation of strain data simpler; the strain history is simply extracted from the neck area, which is approximately the same as extraction of the max strain values. Figure 6 shows a series of strain fields present on a typical PC specimen stretched at the intermediate rate.

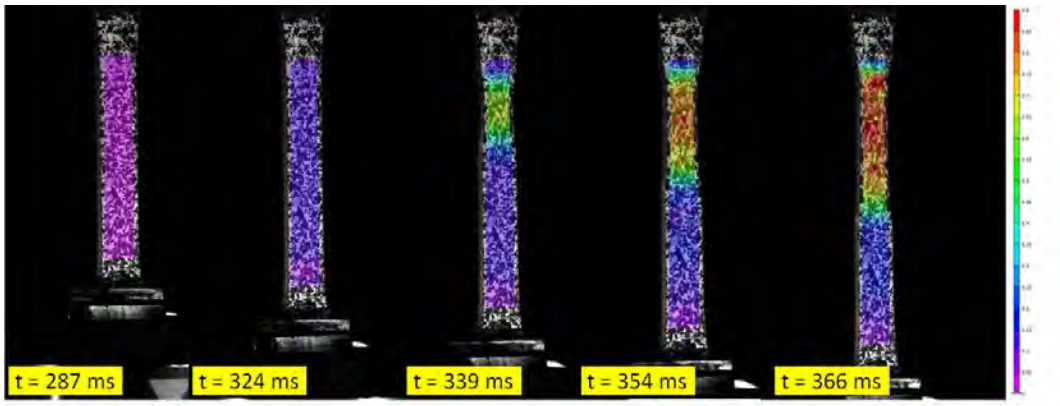


**Fig. 6 Mechanical response of PC specimen at intermediate rate**

Figure 7a shows the strain histories for PC at the intermediate rate, again extracted as an average over the gage length (to make strain rate measurements and allow for comparison with other research) as well as the neck/max strain. The strain rate is approximated from the averaged gage length strain history during the post-yield response, as this is the focus of this research, and is approximately 5/s. The initial linear strain rate from the max during the beginning of necking (0.37–0.40 s) was approximately 10/s and then slowed to 2/s (>0.40 s). Figure 7b shows the strain histories combined with the loading histories to display the mechanical response of PC at the intermediate rate. The max response again shows less softening than the gage length response. However, the softening reduction was not as large as the reduction for the quasi-static rate. The softening for the gage length was 15 MPa, or 18% of the yield stress (82 MPa). The softening for the maximum was 10 MPa, or 12% of the yield stress.

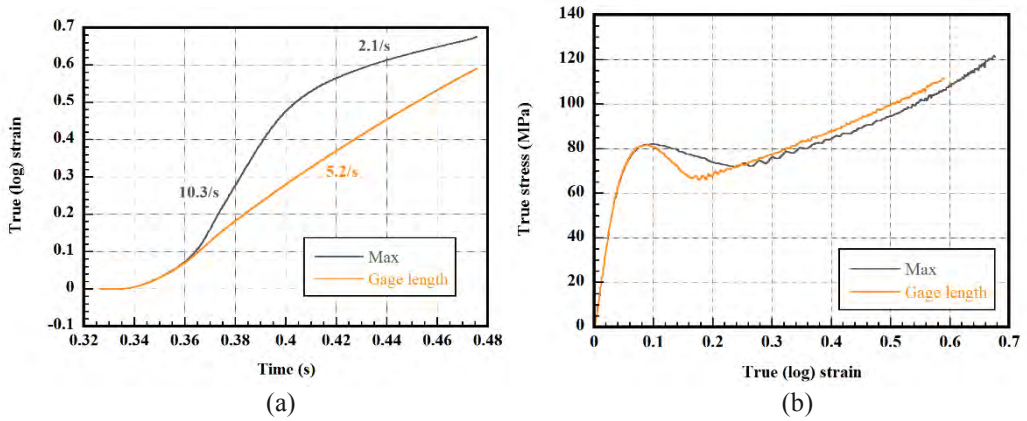


**Fig. 7 Intermediate a) strain histories for max and gage length and b) stress-strain behavior of PC at intermediate rate for max and gage length**

## 3.4 Rate Effects on Mechanical Behavior

The response of PC at the intermediate rate was significantly different from the quasi-static rate; this material has been shown to be highly sensitive to strain rate, demonstrating a significant change in response to even small (1 or 2 orders of magnitude) changes in strain rate. The yield stress increased from 66 MPa at the quasi-static strain rate to 82 MPa at the intermediate strain rate. The material response at the intermediate strain rate continued to be about 15–20 MPa higher for the post-yield behavior, as the material strain hardened and failed. The modulus remained the same at 1.9 GPa for both strain rates. These differences in response to strain rate are shown in Fig. 8, comparing the mechanical response of PC at both tested strain rates.

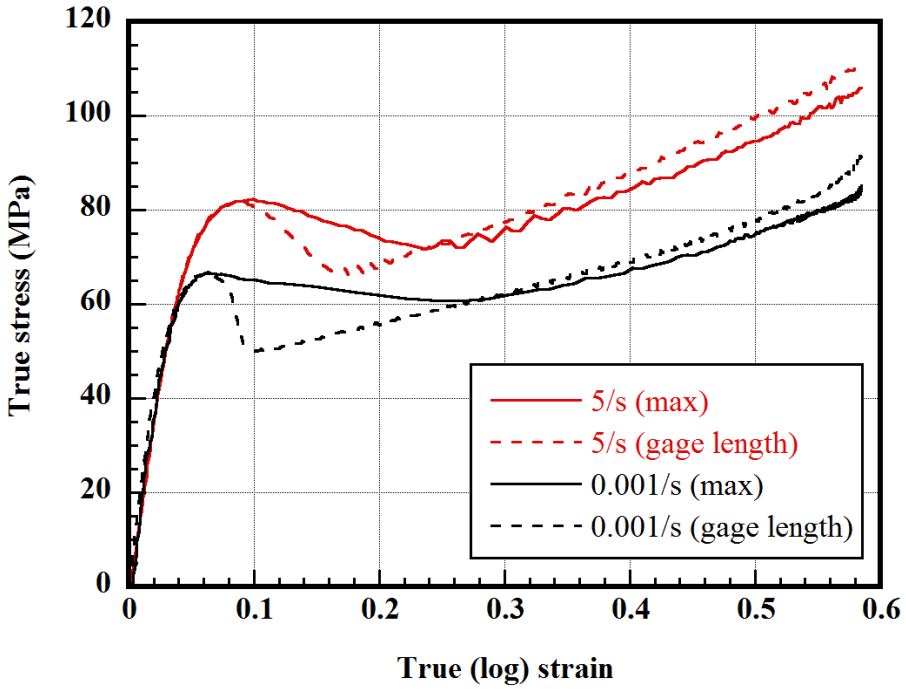


**Fig. 8 Mechanical response at quasi-static and intermediate strain rate for PC**

## 3.5 Thermal Behavior

At quasi-static strain rate (0.001/s), there was evidence of heat generation due to temperature increases measured during the experiments. Figure 9a shows a series of thermal images of the specimen at the same discrete times as the prior strain distribution image series (Fig. 2b). The specimen begins heat generation just as the neck begins to form. The temperature in the neck increased quickly and then reached a constant level. The heat generation then spread out across the gage length, just as the neck "spread" across the gage length.

The maximum temperature change in the gage length is shown in Fig. 9b along with the max strain history. There is no change in temperature until the neck forms, at which point the temperature increases significantly. Once the neck is formed and begins to spread, however, the temperature change levels off and remains constant, having risen 8 °C. This figure shows the delta, or change, in max temperature in the gage length. The rate of temperature increase during the brief period of neck formation (~90–110 s in Fig. 9b) was approximately 0.5 °C/s.

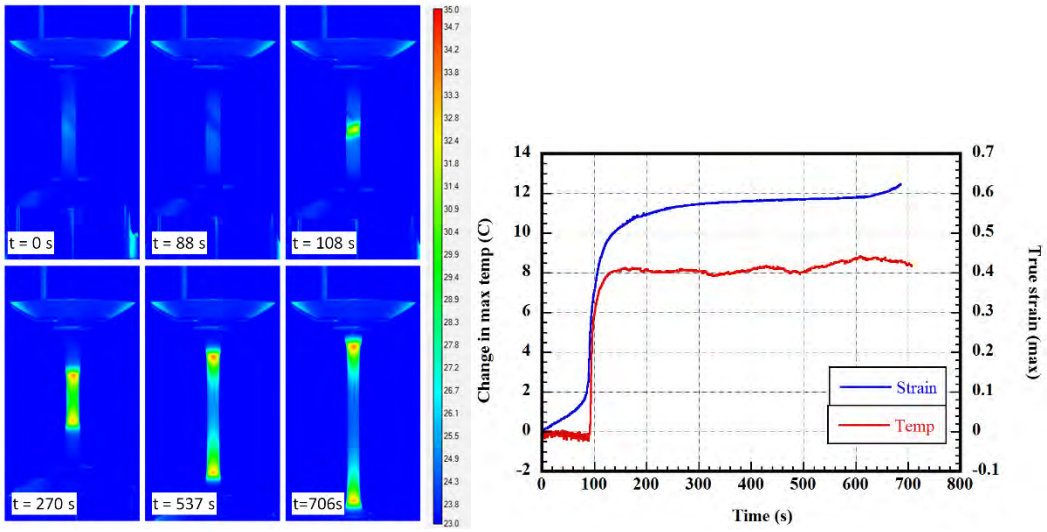


**Fig. 9 Quasi-static a) thermal distribution and b) temperature and strain history at 0.001/s for PC**

It is possible to extract temperature and strain data as a function of position along the specimen gage length. Figure 10 shows the a) strain profiles and b) temperature profiles along the gage length at several discrete times throughout a quasi-static experiment. These profiles can be used to understand quantitatively how the strain and temperature distributions evolve as the specimen is deforming. The times shown in Figs. 10a and 10b are the same times used for the strain and thermal distributions in Figs. 2b and 9a: 0, 88, 108, 270, 537, and 706 s. The location of 0 mm in Figs. 10a and 10b corresponds to the approximate bottom of the gage length when the specimen is undeformed. As the specimen stretches, the gage length gets longer, which is shown by the profiles extending into negative locations at the later times.

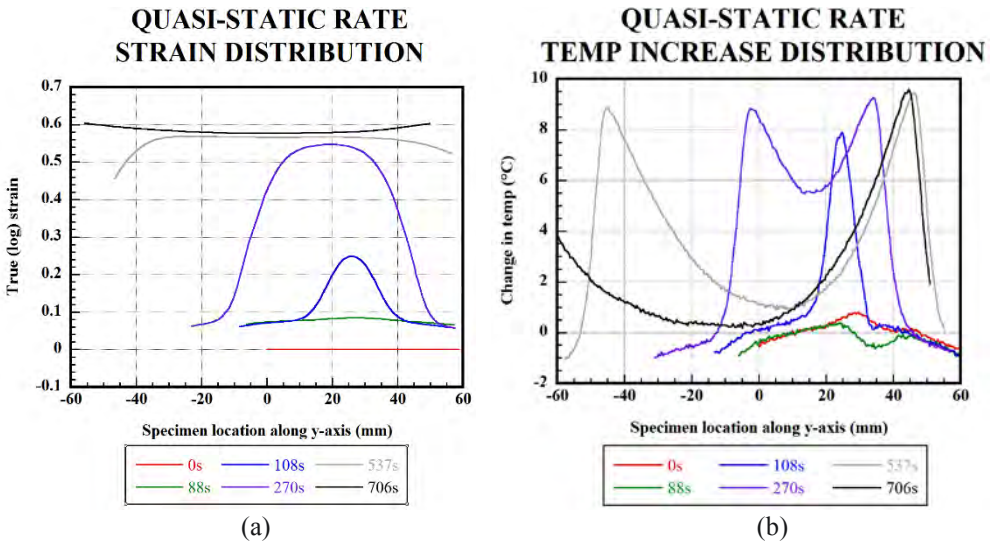


**Fig. 10 Distribution profiles along the gage length for PC at quasi-static rate for a) strain and b) temperature change**

At 0 s, the temperature increase should be zero across the specimen; due to the sensitivity of the IR camera to ambient reflected IR energy (light), the specimen is not at a single temperature but rather has a distribution that varies along the gage length of ±0.5 °C. At 88 s, which corresponds to approximately the end of elastic loading, the specimen strain has increased a constant amount along the gage length while the temperature has not increased at all. At 108 s, the neck has begun to form, and this can be seen in the strain localization as well as the sharp temperature increase localization. At 270 s, the neck has reached its maximum strain and has spread along approximately half the gage length. The temperature maximum is occurring at the "neck fronts", while the location where the neck originally began to form has already begun to cool off. At 537 and 706 s, it is shown that the neck and temperature maximum locations have spread farther away from the gage length center. Failure occurs at approximately the –55 mm location.

It is likely that at these low strain rates some of the heat generated during plastic strain is being lost to cooling. The rate of heat generation may be close to the rate of cooling that occurs during convection between the specimen and laboratory atmosphere and conduction between the specimen and grips. A pair of experiments from the intermediate rate data set was used to understand the cooling behavior of these specimens when located in the experimental setup. After being heated (by stretching at the intermediate rate to failure), 2 specimens were observed as they cooled for the first few minutes after the test. Figure 11 shows the maximum temperature in the specimen after failure as it cooled postexperiment. As can be seen from the data, the specimens cooled via conduction and convection in the test fixtures at a rate of approximately 0.04–0.06 °C/s. Of course, these cooling

estimates are only valid over the limited temperature range seen here, approximately 25–50 °C, as well as for the grips and testing setup used. Still, it is likely that the rate of temperature increase during plastic strain, even at the quasi-static strain rate, is much higher that the cooling rate, such that the effect of cooling during the experiment may be assumed negligible.

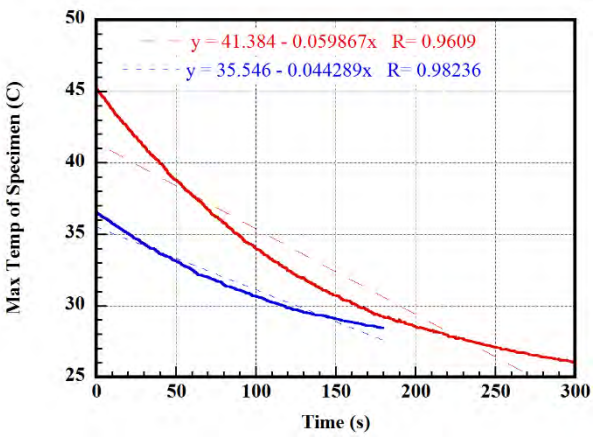


**Fig. 11 Cooling response of PC specimens after failure**

The PC exhibited a significant amount of heat generation that was measured as temperature increase of the specimen when stretched at the intermediate strain rate (~5/s). This heating is generated mostly during plastic deformation as the long molecular chains slide along one another creating friction and heat. Figure 12 shows the maximum specimen temperature increase during deformation as well as the strain history of the PC at both the a) quasi-static rate (repeated from Fig. 9b with matched y-scales for ease of comparison) and b) intermediate rate. The temperature begins to increase as the plastic deformation begins. Just as with the quasi-static rate, the temperature increase was concentrated at the location of the neck. At the intermediate rate, the maximum change in temperature was approximately 28 °C, more than triple the maximum temperature increase at the quasi-static rate (8 °C). The rate of temperature increase is not very linear; at the time of initial necking (0.37–0.38s), the temperature is increasing at a rate of approximately 820 °C/s, while afterward, from 0.38 s to failure (0.405s), the change in temperature slows to a rate of approximately 375 °C/s.

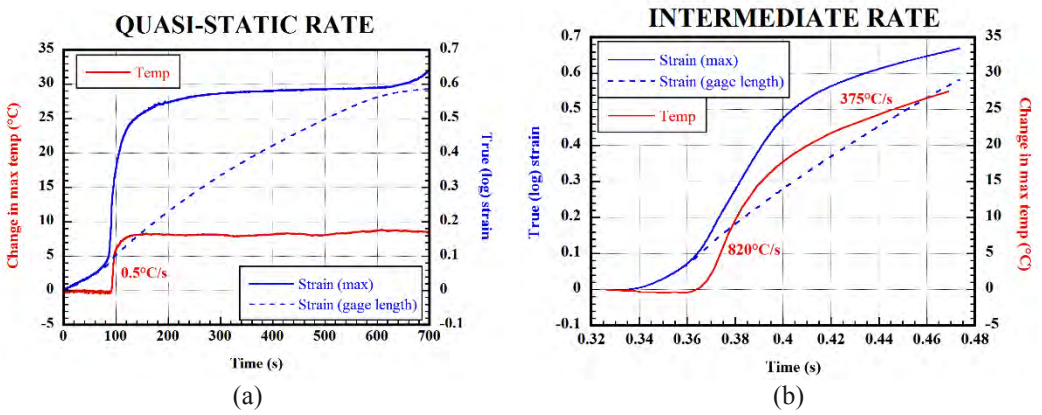


**Fig. 12 Maximum temperature change and strain histories for PC at a) quasi-static and b) intermediate rates**

It is also useful to understand how the heat generated during deformation is related to the amount of strain or deformation. Figure 13 shows the specimen temperature increase as a function of the strain history of PC at both a) the quasi-static rate and b) intermediate rate. Both results show no heat generation during the initial strain generated during elastic loading up until yield. After necking occurs and the strain begins to localize, both rates show a substantial increase of temperature due to strain localization. The intermediate rate shows a constant rate of temperature increase (47.4 °C/ε) across the entire plastic strain region ($\varepsilon > 0.1$). The quasi-static rate actually demonstrates a higher initial rate of temperature increase (64.5 °C/ε) from $0.25 < \varepsilon < 0.35$ than the intermediate rate. This slows to 13.8°C/ε during the strain region of $0.35 < \varepsilon < 0.50$.

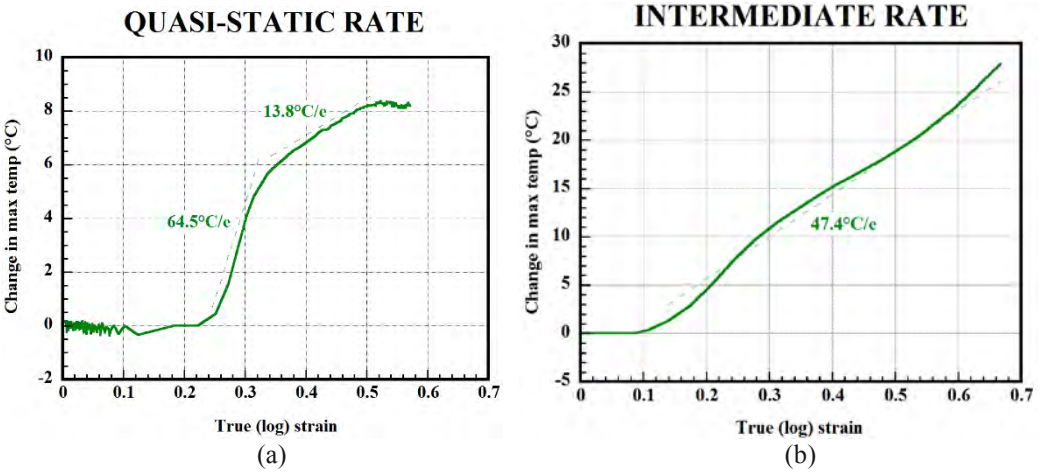


**Fig. 13 Maximum temperature change as a function of max strain for PC at a) quasi-static rate and b) intermediate rate**

## 4. Conclusions

A technique was developed to enable measurement of the mechanical and thermal response of polymers, and specifically PC, at quasi-static to intermediate strain rates using a standard polymer test specimen geometry. PC is highly rate-sensitive with significant changes in response to increasing in strain rate. The yield stress and tensile strength both increased as strain rate increased while the modulus remained constant. At both strain rates, there was a significant amount of adiabatic heat generation observed during plastic deformation; this heating contributes to the softening of the response of PC after yield. Increased strain rate also increased the amount of heat generated; the temperature increase in the specimen at the neck more than tripled as the strain rate increased from quasi-static to intermediate. This data will be used to help develop and refine models that are used to simulate this material.

## 5. References


1. Myers FS, Brittain JO. Mechanical relaxation in polycarbonate-polysulfone blends. Journal of Applied Polymer Science. 1973;17:2715–2724.
2. Petersen RJ, Corneliussen RD, Rozelle LT. Polymer Reprint. 1969;10:385.
3. McNaught AD, Wilkinson A, editors. IUPAC compendium of chemical terminology. Zurich (Switzerland): International Union of Pure and Applied Chemistry; 1997. p. 583.
4. Lo YC, Halldin GW. The effect of strain rate and degree of crystallinity on the solid-phase flow behavior of thermoplastic. In: ANTEC 84. Proceedings of the 42nd Technical Conference and Exhibition; 1984 Apr 30–May 3; New Orleans, LA. Bethel (CT): Society of Plastics Engineers; c1984. p. 488–491.
5. Kaufman HS. Introduction to polymer science and technology. New York (NY): John Wiley and Sons; 1977.
6. Moy P, Weerasooriya T, Hsieh A, Chen W. Strain rate response of a polycarbonate under uniaxial compression. Proceedings of the SEM Annual Conference on Experimental Mechanics; 2003 June 2–4; Charlotte, NC.
7. Mulliken AD, Boyce MC. Mechanics of rate-dependent elastic-plastic deformation of glassy polymers from low to high strain rates. Int J Solids Struct. 2006;43(5):1331–1356.
8. Hall IH. The effect of strain rate on the stress-strain curve of oriented polymers. II. The influence of heat developed during extension. Journal of Applied Polymer Science. 1968;12:739.
9. Walley SM, Field JE, Pope PH, Stafford NA. A study of the rapid deformation behavior of a range of polymers. Philos Trans Soc London A. 1989;328:783–811.
10. Arruda EM, Boyce MC, Jayachandran R. Effects of strain rate, temperature, and thermomechanical coupling on the finite strain deformation of glassy polymers. Mechanics of Materials. 1995;19:193–212.
11. Boyce MC, Arruda EM, Jayachandran R. The large strain compression, tension, and simple shear of polycarbonate. Polymer Engineering and Science. 1994;34(9):716–725.
12. Boyce MC, Sarva SS. Mechanics of polycarbonate during high-rate tension. Journal of Mechanics of Materials and Structures. 2007;2(10):1853–1880.

13. Chu TC, Ranson WF, Sutton MA, Peters WH. Applications of digital-image-correlation techniques to experimental mechanics. Experimental Mechanics. 1985;25(3):232–244.

14. Sutton MA, Wolters WJ, Peters WH, Ranson WF, McNeill SR. Determination of displacements using an improved digital image correlation method. Computer Vision. 1983;1(3):133–139.

15. Bruck HA, McNeill SR, Russell SS, Sutton MA. Use of digital image correlation for determination of displacements and strains. In: Workman GI, editor. Non-destructive evaluation for aerospace requirements. New York (NY): Gordon and Breach; 1989. p. 99–111.

16. Sutton MA, McNeill SR, Helm JD, Schreier H. Full-field non-contacting measurement of surface deformation on planar or curved surfaces using advanced vision systems. ATEM ’99. Proceedings of the International Conference on Advanced Technology in Experimental Mechanics; 1999 July; Tokyo, Japan.

17. Sutton MA, McNeill SR, Helm, Chao YJ. Advances in two-dimensional and three-dimensional computer vision. Photomechanics. 2000;77:323-372.

18. ASTM D638-10. Standard test method for tensile properties of plastics. West Conshohocken (PA): ASTM International; 2010.

## List of Symbols, Abbreviations, and Acronyms

| | |
|---|---|
| ASTM | American Society for Testing and Materials |
| DIC | digital image correlation |
| IR | infrared |
| max | maximum |
| PC | polycarbonate |
| PMMA | poly(methyl methacrylate) |
| $T_G$ | glass transition temperature |

1 (PDF) DEFENSE TECHNICAL INFORMATION CTR
DTIC OCA

2 (PDF) DIRECTOR
US ARMY RESEARCH LAB
RDRL CIO LL
IMAL HRA MAIL & RECORDS MGMT

1 (PDF) GOVT PRINTG OFC
A MALHOTRA

1 (PDF) DEPARTMENT OF ENGINEERING SCIENCE AND MECHANICS
VIRGINIA POLYTECHNIC INSTITUTE AND STATE UNIVERSITY
ROMESH BATRA

1 (PDF) WHITING SCHOOL OF ENGINEERING
JOHNS HOPKINS UNIVERSITY
VICKY NGUYEN

88 (PDF) DIRECTOR
US ARMY RESEARCH LAB
RDRL CI
P PLOSTINS
RDRL WM
P BAKER
B FORCH
S KARNA
J MCCAULEY
RDRL WML
M ZOLTOSKI
RDRL WML A
W OBERLE
RDRL WML F
G BROWN
RDRL WML G
J SOUTH
RDRL WML H
T EHLERS
L MAGNESS
C MEYER
J NEWILL
D SCHEFFLER
B SCHUSTER
RDRL WMM
J BEATTY
B DOWDING
RDRL WMM A
D O'BRIEN
E WETZEL
RDRL WMM B
M FOSTER
G GAZONAS
D GRAY
R KASTE
B LOVE
P MOY
T WALTER
V WU
C YEN
RDRL WMM C
A BUJANDA
R JENSEN
J LA SCALA
RDRL WMM D
R CARTER
B CHEESEMAN
E CHIN
Y HUANG
S WALSH
W ZIGLER
RDRL WMM E
G GILDE
J LASALVIA
P PATEL
J SINGH
J SWAB
RDRL WMM F
S GRENDAHL
L KECSKES
RDRL WMM G
J LENHART
K MASSER
R MROZEK
A RAWLETT
K STRAWHECKER
RDRL WMP
S SCHOENFELD
RDRL WMP B
S ALEXANDER
A DAGRO
A DILEONARDI
A GUNNARSSON
C HOPPEL
M LYNCH
S SATAPATHY
A SOKOLOW
M SCHEIDLER
T WEERASOORIYA
T ZHANG
RDRL WMP C
R BECKER
S BILYK
T BJERKE
J BRADLEY
D CASEM

J CLAYTON
M FERMEN-COKER
M GREENFIELD
B LEAVY
C MEREDITH
C WILLIAMS
RDRL WMP D
R DONEY
D KLEPONIS
C RANDOW
J RUNYEON
S SCHRAML
B SCOTT
RDRL WMP E
S BARTUS
M BURKINS
D HACKBARTH
E KLIER
RDRL WMP F
E FIORAVANTE
N GNIAZDOWSKI
R GUPTA
R KARGUS
RDRL WMP G
N ELDREDGE
RDRL WMS
M VANLANDINGHAM